Calculations on critical points under Gaussian blurring

A. Kuijper, L. M. J. Florack

UU-CS-1999-12

Calculations on Critical Points under Gaussian Blurring

Arjan Kuijper and Luc Florack

Utrecht University, Department of Computer Science
Padualaan 14
NL-3584 CH Utrecht, The Netherlands

arjan@cs.uu.nl, florack@cs.uu.nl

Abstract. The behaviour of critical points of Gaussian scale-space images is mainly described by their creation and annihilation. In existing literature these events are determined in so-called canonical coordinates. A description in a user-defined Cartesian coordinate system is stated, as well as the results of a straightforward implementation. The location of a catastrophe can be predicted with subpixel accuracy. An example of an annihilation is given. Also an upper bound is derived for the area where critical points can be created. Experimental data of an MR, a CT, and an artificial noise image satisfy this result.

1 Introduction

One way to understand the structure of an image is to embed it in a one-parameter family. In this way the image can be endowed with a topology. If a scale-parametrised Gaussian filter is applied, the parameter can be regarded as the "scale" or the "resolution" at which the image is observed. The resulting structure has become know as linear Gaussian scale-space. In view of ample literature on the subject we will henceforth assume familiarity with the basics of Gaussian scale-space theory [4, 8, 9, 14, 22, 23, 25, 28, 29]. In their original accounts both Koenderink as well as Witkin proposed to investigate the "deep structure" of an image, *i.e. structure at all levels of resolution simultaneously*. Encouraged by the results in specific image analysis applications an increasing interest has recently emerged trying to establish a generic underpinning of deep structure. Results from this could serve as a common basis for a diversity of multiresolution schemes. Such bottom-up approaches often rely on *catastrophe theory* [1, 6, 24, 26, 27], which is in the context of the scale-space paradigm now fairly well-established.

The application of catastrophe theory in Gaussian scale space has been studied *e.g.* by Damon [3]—probably the most comprehensive account on the subject—as well as by others [7, 10–13, 15–22]

Closely related to the present article is the work by Florack and Kuijper [5], introducing new theoretical tools. We will summarise their results in section 2 and give an experimental verification of the theory on both real and artificial data sets in section 3. This verification includes visualisation of several theoretical aspects applyed on an MR, a CT, and an artificial noise image. Furthermore we show that the location of a catastrophe can be predicted with subpixel accuracy. Of special interest are creations. We will show experimentally and theoretically that the area where they can occur is small.

2 Theory

The behaviour of critical points as change of the (scale) parameter is described by catastrophe theory. As the parameter changes continuously, the critical points move along critical curves. If the determinant of the Hessian does not become zero, these critical points are called *Morse critical points*. In a typical image these points are extrema (minima and maxima) and saddles. *The Morse lemma* states that the neighbourhood of a Morse critical point can essentially be described by a second order Taylor expansion. At isolated points on a critical curve the determinant of the Hessian may become zero. These points are called *non-Morse points*. Neighbourhoods of such points need a third or higher order Taylor expansion, as described by *Thom's theorem*. If an image is slightly perturbed, the Morse critical points may undergo a small displacement, but nothing happens to them qualitatively. A non-Morse point however will change. In general it will split into a number of Morse critical points. This event is called *morsification*. Thom's theorem give a list of elementary catastrophes with canonical formulas for the catastrophe germs and the perturbations. The Thom splitting lemma states that there exist *canonical coordinates* in which these events can be described. These coordinates however do not coincide with the user-defined coordinates, but are used for notational convenience. In Gaussian scale space the only generic events are *annihilations* and *creations* of a pair of Morse points: an extremum and a saddle. All other events can be split into a combination of one of these events and one 'in which nothing happens'. See Damon [3] for a proof. Canonical descriptions of these events are given by the following formulae:

$$f^{\mathrm{A}}(x, y; t) \stackrel{\mathrm{def}}{=} x^3 + 6xt \pm (y^2 + 2t) \tag{1}$$

$$f^{\mathrm{C}}(x, y; t) \stackrel{\mathrm{def}}{=} x^3 - 6x(y^2 + t) \pm (y^2 + 2t). \tag{2}$$

Note that Eq. (1) and Eq. (2), describing annihilation and creation respectively, satisfy the diffusion equation

$$\frac{\partial u}{\partial t} = \Delta u \,. \tag{3}$$

Here Δ denotes the Laplacean operator. The reader can easily verify that the the form $f^{\mathrm{A}}(x, y; t)$ correspond to an annihilation via the critical path $(\sqrt{-2t}\,,\, 0\,,\, t)\;,\; t \leq 0$ at the origin, whereas $f^{\mathrm{C}}(x, y; t)$ corresponds to a creation at the origin via the critical path $(\sqrt{+2t}\,,\, 0\,,\, t)\;,\; t \geq 0$.

In general the user-defined coordinates will not equal the canonical coordinates. Therefore in general one needs a so-called covariant formalism, in which results are stated in an arbitrary coordinate system. Then the first order approximation of a non-Morse point is given by the linear system

$$\begin{bmatrix} \mathbf{H} & \mathbf{w} \\ \mathbf{z}^{\mathrm{T}} & \mathrm{c} \end{bmatrix} \begin{bmatrix} \mathbf{x} \\ t \end{bmatrix} = - \begin{bmatrix} \mathbf{g} \\ \det \mathbf{H} \end{bmatrix} \,, \tag{4}$$

in which the coefficients are determined by the first order derivatives of the image's gradient $\mathbf{g}$ and Hessian determinant $\det \mathbf{H}$, evaluated at the point of expansion near the critical point of interest $(\mathbf{x}_0\,,\, t_0)$, as follows:

$$\mathbf{H} = \nabla \mathbf{g}\,, \mathbf{w} = \partial_t \mathbf{g}\,, \mathbf{z} = \nabla \det \mathbf{H}\,, \mathrm{c} = \partial_t \det \mathbf{H}\,. \tag{5}$$

See Florack and Kuijper [5] for more details. In 2D images, where $\mathbf{x} = (x\,,\,y)$, this becomes

$$\mathbf{H} = \begin{bmatrix} L_{xx} & L_{xy} \\ L_{xy} & L_{yy} \end{bmatrix} , \tag{6}$$

$$\mathbf{w} = \begin{bmatrix} \Delta L_x \\ \Delta L_y \end{bmatrix} , \tag{7}$$

$$\mathbf{z} = \begin{bmatrix} L_{xxx}L_{yy} + L_{xx}L_{xyy} - 2L_{xy}L_{xxy} \\ L_{yyy}L_{xx} + L_{yy}L_{xxy} - 2L_{xy}L_{xyy} \end{bmatrix} , \tag{8}$$

and

$$\mathrm{c} = L_{xx}\Delta L_{yy} - 2L_{xy}\Delta L_{xy} + L_{yy}\Delta L_{xx}\,. \tag{9}$$

Apparently the first order scheme requires spatial derivatives up to *fourth* order. These derivatives are obtained at any scale by linear filtering:

$$\frac{\partial^{m+n} u(x,y;\sigma)}{\partial x^m\,\partial y^n} \stackrel{\mathrm{def}}{=} (-1)^{m+n} \int u(x',y') \frac{\partial^{m+n}\phi(x'-x,y'-y;\sigma)}{\partial x'^m\,\partial y'^n} dx'dy' \;\;,$$

where $u(x,y)$ is the input image and $\phi(x,y;\sigma)$ a normalised Gaussian of scale σ. It has been shown by Blom [2] that we can take derivatives up to fourth order without problems with respect to the results. It is important to note that Eqs. (4–9) hold *in any Cartesian coordinate system*. This property of form invariance is known as *covariance*.

At Morse critical points it is sufficient to restrict ourselves to $\mathbf{H}\mathbf{x} + \mathbf{w}t = -\mathbf{g}$. The solution is easily found to be

$$\mathbf{x} = -\mathbf{H}^{\mathbf{inv}}\mathbf{g} - \mathbf{H}^{\mathbf{inv}}\mathbf{w}t. \tag{10}$$

If we define $t \stackrel{\mathrm{def}}{=} \det\mathbf{H}\tau$, Eq. (10) becomes $\mathbf{x} = -\mathbf{H}^{\mathbf{inv}}\mathbf{g} - \widetilde{\mathbf{H}}\mathbf{w}\tau$, where the matrix $\widetilde{\mathbf{H}}$ is the transposed cofactor matrix, defined by $\mathbf{H}\widetilde{\mathbf{H}} = \det\mathbf{H}\,\mathbf{I}$. In 2D $\widetilde{\mathbf{H}}$ reads

$$\widetilde{\mathbf{H}} \stackrel{\mathrm{def}}{=} \begin{bmatrix} L_{yy} & -L_{xy} \\ -L_{xy} & L_{xx} \end{bmatrix} . \tag{11}$$

Note that $\widetilde{\mathbf{H}}$ exists even if $\mathbf{H}$ is singular. At critical points the *scale-space velocity* is defined by

$$\overline{\mathbf{w}} \stackrel{\mathrm{def}}{=} -\widetilde{\mathbf{H}}\mathbf{w}\,. \tag{12}$$

Instead of tracing the two branches of the critical curve it is parametrised by a continuous function that is non-degenerate at the catastrophe point. Note that the *scale-space velocity* has the direction of $\overline{\mathbf{w}}$ at extrema and is opposite at saddles.

At non-Morse critical points the determinant of $\mathbf{H}$ becomes zero and we need to invert the complete linear system, Eq. (4). If we define

$$\mathbf{M} \stackrel{\mathrm{def}}{=} \begin{bmatrix} \mathbf{H} & \mathbf{w} \\ \mathbf{z}^{\mathrm{T}} & \mathrm{c} \end{bmatrix} , \tag{13}$$

the solution of Eq. (4) becomes

$$\begin{bmatrix} \mathbf{x} \\ t \end{bmatrix} = -\mathbf{M}^{\text{inv}} \begin{bmatrix} \mathbf{g} \\ \det \mathbf{H} \end{bmatrix} , \tag{14}$$

In general this inverse matrix exists even if the Hessian is singular. Florack and Kuijper [5] have proven that at annihilations $\det \mathbf{M} < 0$ and at creations $\det \mathbf{M} > 0$, where

$$\det \mathbf{M} = \mathrm{c} \det \mathbf{H} + \mathbf{z}^{\mathrm{T}} \overline{\mathbf{w}}. \tag{15}$$

At catastrophes $\det \mathbf{H} = 0$, so Eq. (15) reduces to

$$\det \mathbf{M} = \mathbf{z}^{\mathrm{T}} \overline{\mathbf{w}}, \tag{16}$$

which is the innerproduct between the spatial derivative of $\det \mathbf{H}$, Eq. (5), and the scale-space velocity $\overline{\mathbf{w}}$, Eq. (12). In the next section we will apply these results on several images.

3 Experimental results

In our experiments we used a 64 x 64 subimage of a 256 x 256 MR scan (Fig. 1a and b), CT scan (Fig. 1c and d), and a 64 x 64 artificial image with Gaussian noise of mean zero and standard deviation $\sigma = 10$, also denoted as N(0,10) (Fig. 1e).

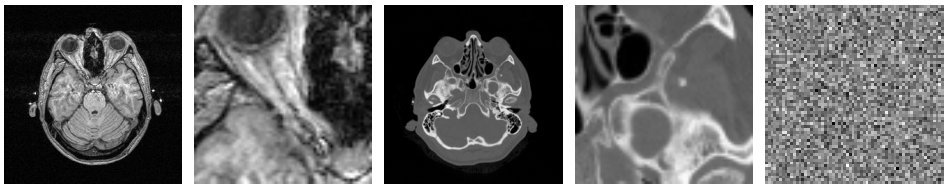

Fig. 1. a) Original 256 x 256 pixel MR image. b) 64 x 64 pixel subimage of a). c) original 256 x 256 pixel CT image. d) 64 x 64 pixel subimage of c). e) 64 x 64 artificial Gaussian N(0,10) noise image.

3.1 Visualisation of $\mathbf{z}^{\mathrm{T}}$ and $\overline{\mathbf{w}}$

At scale $\sigma = 2.46$ the critical points of the MR image (Fig. 1b) are shown in Fig. 2a. Extrema (saddle points) are visualised by the white (black) dots. At the upper middle part of this image a critical isophote generated by a saddle and enclosing two extrema is shown (see also Fig. 2b). At a larger scale the saddle point will annihilate with the upper one of these extrema. We have calculated the direction and magnitude of the vectors $\overline{\mathbf{w}}$ (see Eq. (12)) and $\mathbf{z}^{\mathrm{T}}$ (see Eq. (5)) and show them on the two critical points at two subsequent scales $\sigma = 2.46$ and $\sigma = 2.83$ in Fig. 2c and d, respectively. Indeed the velocity (given by $\overline{\mathbf{w}}$) of the extremum (dark arrow at the white dot) is in the direction

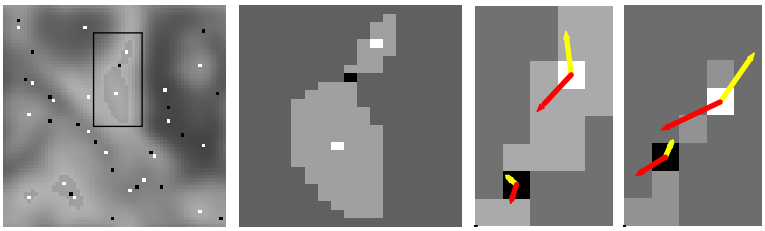

Fig. 2. a) Critical points (extrema white, saddles black) of Fig. 1b at scale $\sigma = 2.46$. At the field of interest the critical isophote through a saddle is shown; b) subimage of a, showing the field of interest more clearly. The saddle is about to annihilate with the upper extremum; c) Subimage of the two annihilating critical points and the vectors of $\overline{\mathbf{w}}$ (dark) and $\mathbf{z}^{\mathrm{T}}$ (bright) at scale $\sigma = 2.46$; d) Same, at scale $\sigma = 2.83$.

of the saddle, and thus in the direction of the point of annihilation. The velocity vector at the saddle has the same direction, as the result of the parametrisation by Eq. (12))

Furthermore since the point where the annihilation takes place (at $\det \mathbf{H} = 0$) is between the two critical points, the vector $\mathbf{z}^{\mathrm{T}}$, which is the normalvector (recall Eq.(5)) to the zero-crossing of $\det \mathbf{H}$, directs from the saddle towards the extremum both at the saddle and the extremum.

Finally it can be seen that the vectors of $\mathbf{z}^{\mathrm{T}}$ and $\overline{\mathbf{w}}$ at the critical points have an angel of more than $\frac{\pi}{2}$. Since $\det \mathbf{M}$ is the innerproduct of these vectors at a catastrophe (see Eq. (16)), this leads to a negative sign of $\det \mathbf{M}$, *i.e.* the two critical points approach each other and disappear eventually.

3.2 Location of the catastrophe

The location of the catastrophe can be found by inverting the linear system, Eq. (4), yielding Eq. (14). The result of 4 subsequent scales for the MR subimage (Fig. 2c) are shown in Fig. 3. The approximate location of the catastrophe can be found with subvoxel precision by averaging the arrows as shown in Table 1. The black dot in Fig. 3 is located at the estimated position of the catastrophe, the ellipse shows the standard deviation of the estimation.

Below the catastrophe-scale the location is accurate whereas at a scale above it (at $\sigma = 3.32$, see Fig. 3d) the estimate location turns out to be more uncertain. The estimation of the t-coordinate is positive below catastrophe-scale and negative above, as expected. The standard deviation is largely influenced by the cells that are distant from the critical curve, which also can be seen in Fig 3d. Since the relation between scale σ and coordinate t is given by $t = \frac{1}{2}\sigma^2$, we can easily calculate the estimated scale $\sigma_{est} = \sqrt{\sigma^2 + 2t_{calc}}$ with error $\delta\sigma_{est} = \partial_t\sigma_{est} \cdot \delta t_{calc} = \delta t_{calc}/\sigma_{est}$.

By slightly increasing scales the catastrophe is found between the scales 3.050 and 3.053, which is covered by all estimated scales in Table 1. Since the estimation is a linear approximation of the top of a curve a small overestimation (*here:* a tenth of a pixel) is expected and indeed found in this case. In summary the location of the catastrophe point can be pinched down by linear estimation with subpixel precision.

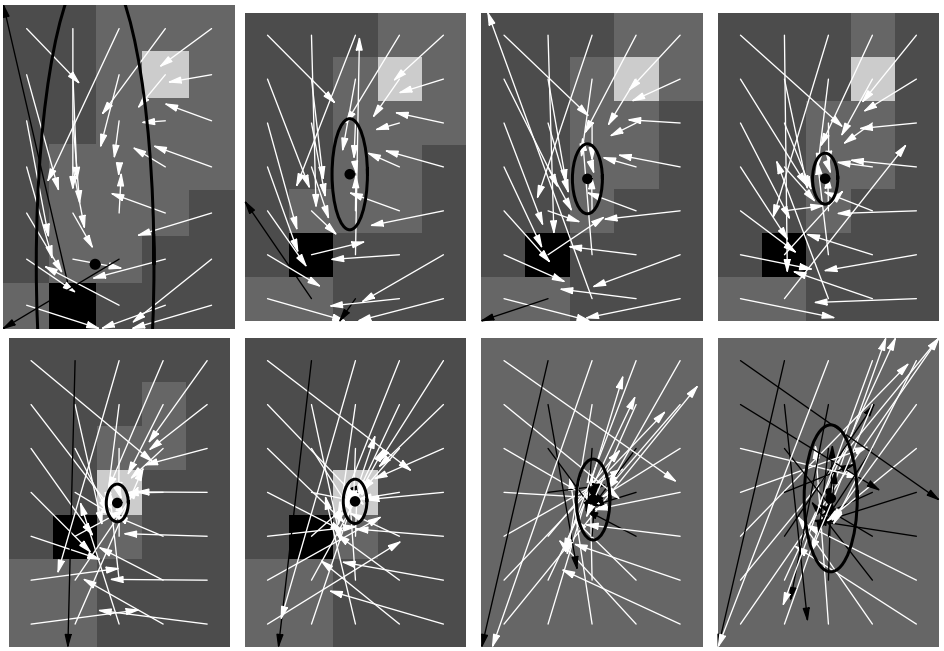

Fig. 3. Visualisation of Eq. (14) of the vector (x, y); a bright (dark) arrow signifies a positive (negative) value of the t-component. The black dot is located at the mean value of the inner 15 arrows, the ellipse shows the standard deviation (see Table 1). First row: a: scale $\sigma = 2.34$; b: scale $\sigma = 2.46$; c: scale $\sigma = 2.59$; d: scale $\sigma = 2.72$. Second row: a: scale $\sigma = 2.86$; b: scale $\sigma = 3.00$; c: scale $\sigma = 3.16$, a catastrophe has occurred; d: scale $\sigma = 3.32$.

scale	x-coordinate	y-coordinate	t-coordinate	estimated scale
2.34	0.481197 ± 1.27275	-0.111758 ± 6.54458	0.630053 ± 3.7568	2.59501 ± 1.4477
2.46	0.869898 ± 0.401954	1.83346 ± 1.26546	1.58998 ± 0.663776	3.03808 ± 0.218489
2.59	0.893727 ± 0.340422	1.72886 ± 0.79602	1.3391 ± 0.447622	3.06008 ± 0.146278
2.72	0.92611 ± 0.286782	1.73222 ± 0.580028	1.10524 ± 0.434127	3.09831 ± 0.140117
2.86	0.95843 ± 0.250132	1.75858 ± 0.429409	0.824525 ± 0.483923	3.13293 ± 0.154464
3.00	0.991123 ± 0.26873	1.79548 ± 0.504445	0.466264 ± 0.597825	3.15556 ± 0.189451
3.16	1.02368 ± 0.380863	1.83618 ± 0.921176	-0.00573945 ± 0.792309	3.15638 ± 0.251019
3.32	1.05174 ± 0.603366	1.86346 ± 1.67306	-0.642702 ± 1.1066	3.12054 ± 0.354618

Table 1. Estimation of the location of the catastrophe, as an avarage of the 15 arrows in the rectangle spanned by the two critical points of Fig. 3a. The origin in the (x, y)-plane is fixed for all figures at the middle of the saddle (black square) of Fig. 3a. The average value of the t-direction is positive below catastrophe scale and negative above it.

3.3 Fraction of the area where $\det \mathbf{M} > 0$

In the following figures we show the percentage of the image where $\det \mathbf{M}$ is larger than zero, *i.e.* the relative area where creations can occur. For the MR image we see a relative area of maximal 0.12 (Fig. 4, top-left). Furthermore the number of critical points decreases logarithmically with scale (Fig. 4, top-right). The slope is $-1.76 \pm .01$. An a priori estimation value is -2, see *e.g.* Florack's monograph [4].

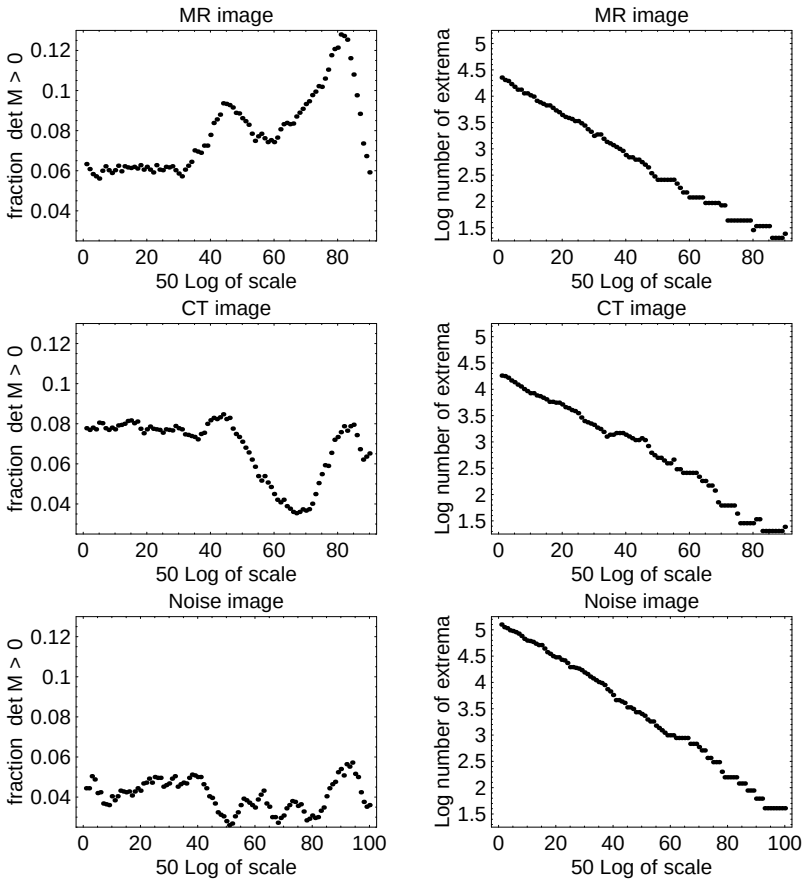

Fig. 4. Results of calculations; scales vary from $e^{1/50}$ to $e^{90/50}$; First row: MR image; Second row: CT image; Third row: artificial noise image. First column: Fraction of $\det \mathbf{M} > 0$, ranging from 0.04 to 0.12 for the MR and CT image, and less for the artifical noise image; Second column: Logarithm of the number of critical points, with slopes $-1.76 \pm .01$, $-1.74 \pm .02$, and $-1.84 \pm .01$, respectively;

In Fig. 5 the image of the sign of $\det \mathbf{M}$ of the MR-subimage (Fig. 1b) is shown at four subsequent scales. It appears that the locations of the image where $\det \mathbf{M}$ is positive are relatively small isolated areas.

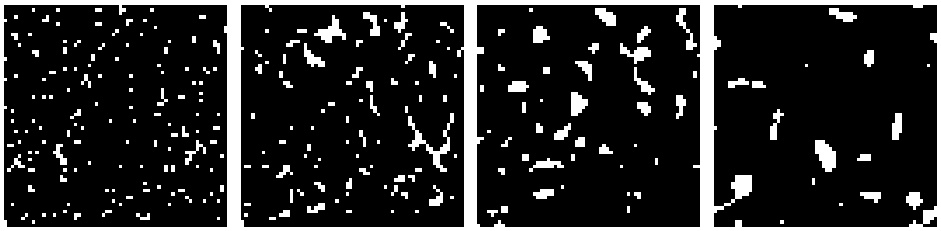

Fig. 5. In white the area where $det\mathbf{M} > 0$ a: at scale $\sigma = 1.57$, corresponding to the value 22.5 on the horizontal axis of Fig. 4 b: at scale $\sigma = 2.46$, (value 45) c: at scale $\sigma = 3.866$, (value 67.5) d: at scale $\sigma = 6.05$, (value 90)

For the CT image we see more or less the same results (Fig. 4, second row): the fraction where $\det \mathbf{M}$ is positive is a bit higher at small scales ($\sigma < 2.22$, the value 40 at the horizontal axis) and a bit smaller at high scales. The slope of graph of the logarithm of the number of critical points at increasing scale is found to be -1.74 ± 0.02. At the noise image the relative area where $\det \mathbf{M} > 0$ is smaller than at the MR and CT images. This might indicate that creations need a global structure (like a bridge), being absent in a noise image. The logarithm of the number of extrema has a slope of $-1.84 \pm .01$ (Fig. 4, bottom-right), which is closer to the expected value -2 than the slope at the MR and CT image. This also might be caused by the lack of structure in the noise image.

3.4 Estimation of the area where $\det \mathbf{M} > 0$

If the Hessian becomes singular, the rows (or, equivalently the columns) are dependent of each other, *i.e.* $(L_{xx}\ ,\ L_{xy}) = \lambda(L_{xy}\ ,\ L_{yy})$. Therefore [1] $L_{xx} = \lambda^2 L_{yy}$ and $L_{xy} = \lambda L_{yy}$. So in general, the Hessian at a catastrophe can be described by

$$\mathbf{H} = \begin{bmatrix} \lambda^2 & \lambda \\ \lambda & 1 \end{bmatrix} L_{yy}\ ,\ \tilde{\mathbf{H}} = \begin{bmatrix} 1 & -\lambda \\ -\lambda & \lambda^2 \end{bmatrix} L_{yy} \tag{17}$$

The second order Taylor expansion of the image now reads $\frac{1}{2}\lambda^2 L_{yy}\, x^2 + \lambda\, L_{yy}\, x\, y + L_{yy}\, y^2$ which reduces to $\frac{1}{2} L_{yy}\, (\lambda\, x + y)^2$. The parameter λ depends on the rotation between the axes of the real and the canonical coordinates. If these coincide we have $\lambda = 0$, i.e. both L_{xx} and L_{xy} are zero, see Eqs.(1) and (2). With Eqs.(7-8), (12), (16-17) the explicit form of $\det \mathbf{M}$ at a catastrophe in 2D reduces to

$$\det \mathbf{M} = L_{yy}^2 (L_{xxx} - 3\lambda L_{xxy} + 3\lambda^2 L_{xyy} - \lambda^3 L_{yyy})(-L_{xxx} + \lambda L_{xxy} - L_{xyy} + \lambda L_{yyy}) \tag{18}$$

Equation (18) can be regarded as the product of two linear planes in the 4-dimensional $(L_{xxx}, L_{xxy}, L_{xyy}, L_{yyy})$ space. The planes divide this space into 4 subspaces where

[1] The choice of L_{yy} as leading term is of minor importance, we could just as well have chosen $\mu(L_{xx}\ ,\ L_{xy}) = (L_{xy}\ ,\ L_{yy})$, leading to $L_{yy} = \mu^2 L_{xx}$ and $L_{xy} = \mu L_{xx}$, which would be particularly prudent if L_{yy} is close to zero.

the determinant is either positive or negative, whereas any point on the planes leads to $\det \mathbf{M} = 0$. The normal vectors to these planes are given by $n_1 = (1, -3\lambda, 3\lambda^2, -\lambda^3)$ and $n_2 = (-1, \lambda, -1, \lambda)$. The factor L_{yy}^2 does not change the sign of the determinant. By definition we then have

$$\cos\phi = \frac{n_1 \cdot n_2}{\|n_1\| \cdot \|n_2\|} = -\frac{1 + 6\lambda^2 + \lambda^4}{\sqrt{(2 + 2\lambda^2)(1 + 9\lambda^2 + 9\lambda^4 + \lambda^6)}} \tag{19}$$

As easily can be seen this angle is invariant with respect to the transformations $\lambda \to -\lambda$ and $\lambda \to \frac{1}{\lambda}$. Fig. 6a shows the cosine of the angle for different values of λ.

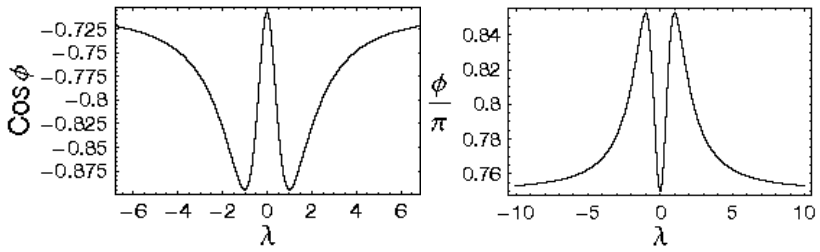

Fig. 6. Left: Cosine of the angle of planes given by Eq. (19). Right: Fraction of the 4D $(L_{xxx}, L_{xxy}, L_{xyy}, L_{yyy})$-space where $\det \mathbf{M}$ is smaller than zero.

Lemma 1. *The fraction of the space where creations can occur is bounded by* $\frac{1}{\pi} \arccos(\frac{2}{5}\sqrt{5}) \approx 0.148\ldots$ *and* $\frac{1}{4}$.

Proof. The fraction of the space where annihilations can occur is given by the fraction of the image where $\det \mathbf{M} < 0$. Since Eq. (19) is negative definite and $\phi \in [0\,,\,\pi]$, the fraction $\frac{\phi}{\pi}$ gives the fraction of the space where annihilations can occur. This fraction varies from $\frac{3}{4}$ at both $\lambda = 0$ and $\lambda \to \infty$, to $\frac{1}{\pi} \arccos(-\frac{2}{5}\sqrt{5}) \approx 0.852\ldots$ at $\lambda = 1$, which follow directly from differentiation, see also Fig. 6b. Equivalently, creations can occur in at most $\frac{1}{4}$ of all possible tupels.

At the usual generic events, *e.g.* discussed by Damon [3] and others [10] only the case $\lambda = 0$ is discussed. They restrict their selves to the canonical coordinates and find Eq.(1) and (2). Then Eq. (18) reduces to $\det \mathbf{M} = -L_{yy}^2\, L_{xxx}\, (L_{xxx} + L_{xyy})$ and it can easily be seen that the fraction of the space is $\frac{3}{4}$, *i.e.* in only $\frac{1}{4}$ of the possible values of L_{xxx} and L_{xyy} a creation can occur.

4 Conclusion and Discussion

We have used an operational scheme to characterise critical points in scale-space. The characteristic local property of a critical point is determined by its Hessian signature

(saddle or extremum). Pairs of critical points with opposite signature can be annihilated or created. Close to such catastrophes, empirically observed properties of the critical points are consistent with the presented theory. The location of catastrophes in scale space can be found with subpixel accuracy. The approximate location of an annihilation and the idea of scale space velocity have been visualised. In general, more annihilations than creations are observed, probably because creations need a special structure of the neighbourhood. This is also indicated by the results of the noise image. We have shown that the area where creations can occur is at most $\frac{1}{4}$. In our experiments this fraction is even smaller than *viz.* $\frac{1}{8}$. In future work we will investigate the correlation between the distributions of the various derivatives in the definition of $\det \mathbf{M}$. Blom [2] has given a general framework, which might give a more precise explanation of the small number of creations.

References

1. V. I. Arnold. *Catastrophe Theory*. Springer-Verlag, Berlin, 1984.
2. J. Blom, B. M. ter Haar Romeny, A. Bel, and J. J. Koenderink. Spatial derivatives and the propagation of noise in Gaussian scale-space. *Journal of Visual Communication and Image Representation*, 4(1):1–13, March 1993.
3. J. Damon. Local Morse theory for solutions to the heat equation and Gaussian blurring. *Journal of Differential Equations*, 115(2):368–401, January 1995.
4. L. M. J. Florack. *Image Structure*, volume 10 of *Computational Imaging and Vision Series*. Kluwer Academic Publishers, Dordrecht, The Netherlands, 1997.
5. L. M. J. Florack and A. Kuijper. On the Behaviour of Critical Points under Gaussian Blurring *Submitted to Scale-Space '99*.
6. R. Gilmore. *Catastrophe Theory for Scientists and Engineers*. Dover Publications, Inc., New York, 1993. Originally published by John Wiley & Sons, New York, 1981.
7. L. D. Griffin and A. C. F. Colchester. Superficial and deep structure in linear diffusion scale space: Isophotes, critical points and separatrices. *Image and Vision Computing*, 13(7):543–557, September 1995.
8. B. M. ter Haar Romeny, L. M. J. Florack, J. J. Koenderink, and M. A. Viergever, editors. *Scale-Space Theory in Computer Vision: Proceedings of the First International Conference, Scale-Space'97, Utrecht, The Netherlands*, volume 1252 of *Lecture Notes in Computer Science*. Springer-Verlag, Berlin, July 1997.
9. T. Iijima. Basic theory on normalization of a pattern (in case of typical one-dimensional pattern). *Bulletin of Electrical Laboratory*, 26:368–388, 1962. (In Japanese).
10. P. Johansen. On the classification of toppoints in scale space. *Journal of Mathematical Imaging and Vision*, 4(1):57–67, 1994.
11. P. Johansen. Local analysis of image scale space. In Sporring et al. [25], chapter 10, pages 139–146.
12. P. Johansen, S. Skelboe, K. Grue, and J. D. Andersen. Representing signals by their top points in scale-space. In *Proceedings of the 8th International Conference on Pattern Recognition (Paris, France, October 1986)*, pages 215–217. IEEE Computer Society Press, 1986.
13. S. N. Kalitzin, B. M. ter Haar Romeny, A. H. Salden, P. F. M. Nacken, and M. A. Viergever. Topological numbers and singularities in scalar images: Scale-space evolution properties. *Journal of Mathematical Imaging and Vision*, 9:253–269, 1998.
14. J. J. Koenderink. The structure of images. *Biological Cybernetics*, 50:363–370, 1984.

15. J. J. Koenderink. The structure of the visual field. In W. Güttinger and G. Dangelmayr, editors, *The Physics of Structure Formation: Theory and Simulation. Proceedings of an International Symposium*, Tübingen, Germany, October 27–November 2 1986. Springer-Verlag.
16. J. J. Koenderink. A hitherto unnoticed singularity of scale-space. *IEEE Transactions on Pattern Analysis and Machine Intelligence*, 11(11):1222–1224, November 1989.
17. J. J. Koenderink. *Solid Shape.* MIT Press, Cambridge, 1990.
18. J. J. Koenderink and A. J. van Doorn. Dynamic shape. *Biological Cybernetics*, 53:383–396, 1986.
19. J. J. Koenderink and A. J. van Doorn. The structure of two-dimensional scalar fields with applications to vision. *Biological Cybernetics*, 33:151–158, 1979.
20. T. Lindeberg. On the behaviour in scale-space of local extrema and blobs. In P. Johansen and S. Olsen, editors, *Theory & Applications of Image Analysis*, volume 2 of *Series in Machine Perception and Artificial Intelligence*, pages 38–47. World Scientific, Singapore, 1992. Selected papers from the 7th Scandinavian Conference on Image Analysis.
21. T. Lindeberg. Scale-space behaviour of local extrema and blobs. *Journal of Mathematical Imaging and Vision*, 1(1):65–99, March 1992.
22. T. Lindeberg. *Scale-Space Theory in Computer Vision.* The Kluwer International Series in Engineering and Computer Science. Kluwer Academic Publishers, 1994.
23. N. Otsu. *Mathematical Studies on Feature Extraction in Pattern Recognition*. PhD thesis, Electrotechnical Laboratory, Ibaraki, Japan, 1981. (In Japanese).
24. T. Poston and I. N. Stewart. *Catastrophe Theory and its Applications.* Pitman, London, 1978.
25. J. Sporring, M. Nielsen, L. M. J. Florack, and P. Johansen, editors. *Gaussian Scale-Space Theory*, volume 8 of *Computational Imaging and Vision Series.* Kluwer Academic Publishers, Dordrecht, 1997.
26. R. Thom. *Stabilité Structurelle et Morphogénèse*. Benjamin, Paris, 1972.
27. R. Thom. *Structural Stability and Morphogenesis (translated by D. H. Fowler)*. Benjamin-Addison Wesley, New York, 1975.
28. J. A. Weickert, S. Ishikawa, and A. Imiya. On the history of Gaussian scale-space axiomatics. In Sporring et al. [25], chapter 4, pages 45–59.
29. A. P. Witkin. Scale-space filtering. In *Proceedings of the International Joint Conference on Artificial Intelligence*, pages 1019–1022, Karlsruhe, Germany, 1983.